THE
AUSTRALIAN
NATIONAL
UNIVERSITY

RESEARCH SCHOOL OF PHYSICAL SCIENCES

ANU-P/1119
February 1993

Spectroscopy Of ^{211}Rn Approaching The Valence Limit

35 p.

P.M. Davidson, G.D. Dracoulis, A.P. Byrne[1], T. Kibédi, B. Fabricius,
A.M. Baxter[2], A.E. Stuchbery, A.R. Poletti[3] and K.J. Schiffer

Department of Nuclear Physics, Research School of Physical Sciences and Engineering
Australian National University, Canberra ACT 0200

1) Department of Nuclear Physics, Research School of Physical Sciences and Engineering and Department of Physics and Theoretical Physics, Faculty of Science, ANU, Canberra ACT 0200
2) Department of Physics and Theoretical Physics, Faculty of Science, ANU, Canberra ACT 0200
(3) Permanent Address: Department of Physics, University of Auckland, Private Bag, Auckland, NZ

INSTITUTE OF ADVANCED STUDIES

Accepted for publication in
Nuclear Physics A, February 1993

SPECTROSCOPY OF ^{211}Rn APPROACHING THE VALENCE LIMIT

P.M. DAVIDSON, G.D. DRACOULIS, A.P. BYRNE[1], T. KIBÉDI, B. FABRICIUS,

A.M. BAXTER[2], A.E. STUCHBERY, A.R. POLETTI[3] and K.J. SCHIFFER

Department of Nuclear Physics, Research School of Physical Sciences and Engineering, Australian National University, GPO Box 4, Canberra, ACT 2601, Australia

Abstract: High spin states in ^{211}Rn were populated using the reaction ^{198}Pt(^{18}O,5n) at 96 MeV. Their decay was studied using γ-ray and electron spectroscopy. The known level scheme is extended up to a spin of greater than 69/2 and many non-yrast states are added. Semi-empirical shell model calculations and the properties of related states in ^{210}Rn and ^{212}Rn are used to assign configurations to some of the non-yrast states. The properties of the high spin states observed are compared to the predictions of the Multi-Particle Octupole Coupling model and the semi-empirical shell model. The maximum reasonable spin available from the valence particles and holes is 77/2 and states are observed to near this limit.

E

NUCLEAR REACTIONS ^{198}Pt(^{18}O,5n), E=96 MeV; measured γγ(t), Eγ, Iγ(E,t), I_{ce}(E,t). ^{211}Rn deduced levels J, π, $T_{1/2}$, ICC. Enriched target, pulsed beam, Ge hyperpure, Compton suppressed detectors. Si(Li), superconducting electron spectrometer.

NUCLEAR STRUCTURE ^{211}Rn, calculated levels, B(λ). Multi-Particle Octupole Coupling model, shell model.

[1] Department of Nuclear Physics, Research School of Physical Sciences and Engineering, and Department of Physics and Theoretical Physics, Faculty of Science, Australian National University, Canberra, ACT 2601, Australia.

[2] Department of Physics and Theoretical Physics, Faculty of Science, Australian National University, Canberra, ACT 2601, Australia.

[3] Permanent Address: Department of Physics, University of Auckland, Private Bag, Auckland, New Zealand.

1. Introduction

The light radon nuclei (Z=86, N = 126) have four protons more than found at the Z=82 shell closure and are close to a complete neutron shell at N=126. As such they are good cases for the application of the nuclear shell model, and in previous publications [1-7]) the structure of the neutron-deficient isotopes has been examined within the framework of that model. In those publications good agreement between calculated and observed energies was attained, but transition strengths were reproduced only after the effect of coupling to the electric octupole collective excitation of the core had been included. This paper reports new experimental information on ^{211}Rn (N=125), extending the level scheme both higher in spin and further from the yrast line. The spectroscopic information which was acquired on weakly populated high-spin and near-yrast states is used, together with the results of the previously published calculations and with the properties of the neighbouring isotopes, to discuss the structure of the states.

Some of the information acquired in this study has been published in a letter [5]) which focussed on the properties of the high spin yrast states. This paper extends that discussion and proposals are advanced about the structure of the highest excited states seen. These are expected to have a spin close to the maximum possible from the available valence particles and holes.

2. Experimental Procedure

The reaction ^{198}Pt (^{18}O,5n) at a beam energy of 96 MeV was used to populate high-spin states in ^{211}Rn. This reaction was relatively free from contaminant products, although a significant amount of ^{210}Rn was formed via the 4n channel. Three types of experiment were performed: a γ–γ coincidence measurement using the Compton suppressed array CAESAR [8]), a beam-pulse–γ-ray timing measurement also using CAESAR (both CAESAR experiments used a 4.0 mg/cm^2 ^{198}Pt enriched foil target), and an electron conversion measurement using a superconducting electron spectrometer [9]). All measurements were made with pulsed beams provided by the ANU 14UD Pelletron accelerator. The pulses had approximately 1 ns duration with approximately 1 μs between pulses. All timing information was with reference to the time of the beam pulse. This

allowed considerable flexibility in the analysis of the γ–γ measurement as either time differences between detected γ-rays or their absolute times after the beam pulse could be used as selection criteria in off-line data analysis.

The analysis of the γ–γ-time coincidence data consisted of the construction of three matrices from the event-mode data. A prompt coincidence matrix was made from γ-ray events that were within 24 ns of one another. An 'early' coincidence matrix was constructed which allowed the generation of spectra corresponding to γ-rays occurring between 24 ns and 812 ns before any selected transition. Similarly, a 'late' coincidence matrix allowed projection of the spectrum of γ-rays occurring between 24 ns and 812 ns after any gating transition. The data from the beam-pulse–γ-ray timing measurement were used to generate a matrix of γ-ray time distributions, from which the lifetimes of isomeric states could be measured.

Anisotropy information was also obtained from the singles yields measured with CAESAR which has six detectors placed in three pairs at ±48°, ±97° and ±145° to the beam axis. An angular distribution coefficient A_2/A_0 was determined assuming, because of the limited number of angles, that the coefficent A_4/A_0 was zero.

Conversion electron measurements were carried out with the electron spectrometer operating in the "LENS" mode described by Kibédi *et al* [9]. A 2.5 mg/cm^2 ^{198}Pt foil target was placed at a steep angle with respect to the beam. The energy resolution obtained was 2.9 keV (FWHM) at 1 MeV. Both a wide range measurement, covering an electron energy range of 100 keV to 1500 keV, and a restricted range measurement (electron energy of 450 keV to 1250 keV) were performed. The restricted range measurement was used to increase the number of events collected over the range of transition energies associated with transitions high in the level scheme. Electrons and γ-rays (measured with a Compton-suppressed Ge detector) were recorded in event mode including their times relative to the pulsed beam. The relative electron-γ-ray efficiency was obtained from source measurements and checked internally using the theoretical values for the conversion coefficients of transitions whose multipolarities had been determined previously [1,2].

The data were sorted into electron-time and γ-ray-time matrices which were transformed to correct for time walk in the respective detectors. Cuts from these matrices then allowed the electron-γ-ray intensity ratios to be determined over specific corresponding time ranges. Owing to the existence of high-spin isomeric states in ^{211}Rn, most of the events of interest were delayed with respect to the beam. Further, the presence of sequences of isomers allowed different parts of the level scheme to be enhanced by selecting appropriately delayed time regions.

3. Results

3.1. LEVEL SCHEME

The level scheme for ^{211}Rn as determined in the present work is shown in figure 1. Table 1 lists all of the γ-rays assigned to ^{211}Rn and their relative intensities and anisotropies. The level scheme has been extended considerably; 27 new levels have been established (in addition to 25 previously known). Between the 860 ns isomer at 1577.8+Δ keV and the 290 ns isomer at 8854.6+Δ′ keV new evidence supporting previously proposed states has been acquired and new states have been placed. Above and feeding the 290 ns isomer, eight new high spin states have been discovered and the lifetime, spin and parity of the state at 9915.5+Δ′ keV have been determined.

Prompt (±24 ns) γ–γ coincidence spectra with gates set on some of the major transitions in the yrast cascade are shown in figure 2. The 569.9 keV transition is in the yrast cascade between isomers at 1577.8+Δ keV and 3926.1+Δ keV which have mean lives of 860 ns and 58 ns respectively. Therefore the spectrum gated on 569.9 keV shows other transitions in cascade between these isomers, the 511.5 keV, 584.2 keV and 601.0 keV transitions as well as the 1068.9 keV transition which is in parallel with the 511.5 keV and 584.2 keV transitions. Also seen are transitions occurring above the 58 ns isomer since a third of the decays from this isomer occur within the 24 ns gating interval.

The prompt coincidence spectrum gated on the 1319.9 keV transition (in the middle panel of figure 2) shows the stronger transitions below the 58 ns isomer at 3926.1+Δ keV and the three transitions immediately above the 20 ns isomer at 5246.0+Δ′ keV, namely the 854.3 keV, 487.8

keV and 366.3 keV transitions. The four strongest transitions above the 41 ns isomer at 6100.3+Δ′ keV (1298.6 keV, 768.7 keV, 687.0 keV and 613.7 keV) are also clearly seen. Some weaker transitions below the 290 ns isomer at 8854.6+Δ′ keV are seen in the prompt spectrum gated on 854.3 keV, the major branch de-exciting the 41 ns isomer at 6100.3+Δ′ keV. In particular, the 146.8 keV, 282.9 keV, 478.0 keV, and 903.7 keV transitions are marked.

Two early spectra (showing γ-rays occurring 24 ns or more before the gating transition) are shown in figure 3, gated on γ-rays placed consecutively in the level scheme. The early spectrum gated on the 854 keV transition shows transitions occurring before the 41 ns isomer at 6100.3+Δ′ keV (see figure 1). The spectrum gated on the 1320 keV transition, which directly follows the 854 keV γ-ray in the level scheme, should show the transitions above the isomer at 6100.3+Δ′ keV as well as any others that feed the 20 ns isomer at 5246.0+Δ′ keV. The lines seen in the 1320 keV gate which do not appear in the 854 keV gate (namely the 366 keV, 488 keV and 854 keV transitions) are placed between the isomers at 5246.0+Δ′ keV and 6100.3+Δ′ keV.

The level scheme determined supports earlier work [2,4]) with the single exception of the 1068.9 keV transition, previously placed high in the level scheme but now located between the $25/2^-$ and $21/2^-$ yrast states. An unseen 27 keV transition is required by this placement. Figure 4 shows the spectrum obtained from a prompt gate set on the 1068.9 keV line, and the difference of the 'early' and 'late' gates for the 1068.9 keV line. The presence in the 'early'–'late' spectrum of all strong lines both below the 860ns isomer and immediately above the 58 ns isomer, in conjunction with the absence of strong 584.2 keV and 511.5 keV lines in the prompt spectrum places the transition unambiguously.

3.1.1. New states below the $63/2^-$ isomer at 8854.6+Δ′ keV. The excitation energies of many previously assigned levels have been independently confirmed by the discovery of other feeding and de-excitation paths. The level at 2114.1+Δ keV is supported by the cascade of the 120.8 keV and 415.4 keV transitions in parallel with the 536.3 keV transition. The level within this cascade at 1698.6+Δ keV could instead be at 1993.2+Δ keV if the order of the two transitions were reversed.

The previously known state at 2650.4+Δ keV (shown on the left hand side of figure 1) is confirmed by the connection to the state at 1577.8+Δ keV via the 1072.6 keV transition and also by a feeding path from the state at 3844.4+Δ keV. Between the states at 3426.3+Δ keV and 2650.4+Δ keV, the lesser intensity of the 308.9 keV transition compared to the 467.0 keV transition between the state at 3426.3+Δ keV and 2650.4+Δ keV suggests the cascade order shown on the level scheme.

A complex pattern of interconnected transitions has been seen parallel to the yrast decay between the states at 5246.0+Δ keV and 3926.1+Δ keV passing through five new states at 4341.2+Δ keV, 4418.1+Δ keV, 4474.0+Δ keV, 4550.9+Δ keV and 4961.0+Δ keV. The position of the state at 4341.2+Δ keV is not certain, possibly being at 4058.8+Δ keV if the feeding and de-exciting transitions were reversed. The other four states have their positions defined by multiple feeding or decay transitions.

The energy of the state at 6714.0+Δ′ keV is confirmed by two additional transitions (880.0 keV and 916.3 keV) feeding it. The 916.3 keV transition is in cascade with a 537.1 keV transition connecting to the state at 8167.6+Δ′ keV, providing additional evidence for this state. The assigned position of the intermediate state in the 916.3 keV / 537.1 keV cascade is supported by a further feeding transition with an energy of 531.6 keV.

The parallel paths between the states at 8328.3+Δ′ keV and 6100.3+Δ′ keV formed by the 1298.6 keV and the new 903.7 keV, 1324.6 keV and 929.4 keV transitions support the positions of both the 7398.9+Δ′ keV and 8328.3+Δ′ keV levels. The position of the level at 7004.0+Δ′ keV depends on the order of the 903.7 keV and 1324.6 keV transitions which is defined by their relative intensities.

3.1.2. New states above the 63/2⁻ isomer at 8854.6+Δ′ keV. One new isomeric state has been discovered at 9915.5+Δ′ keV with a mean life of 13 ns as we have recently reported [5]. Transitions above the 290 ns isomer at 8854.6+Δ′ keV were identified from the early spectra with gates on the 1298.6 keV, 768.7 keV and 687.0 keV transitions. Figure 5 shows the sum of these gates. All lines seen in this spectrum which are also present in each of the individual spectra must

be placed above the 290 ns isomer in ^{211}Rn. However, most of the weaker γ-rays (with less than 15% of the intensity of the 1060.9 keV transition) could not be reliably assigned to particular states. The prompt gate for the 169.8 keV transition shows definite coincidences with 339.9 keV, 896.2 keV and 952.2 keV γ-rays, but the intensities observed make it unlikely that these γ-rays feed the same 170 keV transition. The 896.2 keV prompt gate also shows a 916 keV line. No other coincidence relationships are seen between the unplaced γ-rays.

3.2. CONVERSION COEFFICIENTS

Figure 6 shows out-of-beam (30 ns to 830 ns after the beam pulse) electron and γ-ray spectra. Delayed spectra such as these were used for the determination of conversion coefficients for transitions following the 290 ns isomer. This removed much of the background and a number of the contaminant lines that occurred promptly with the reaction. Table 2 summarizes the electron conversion coefficients obtained for transitions that previously were not assigned a definite multipolarity (see ref [1]) for conversion coefficients measured previously). The results are from the analysis of the wide range conversion electron measurement, except for some lines observed in the restricted range measurement which were weak in the wide range measurement.

In some cases a more comprehensive analysis of timing information assisted the determination of the conversion coefficients. The expected time distributions (obtained from the γ-ray–time information) could be compared with the electron-time spectra, allowing the proportion of contaminants to the intensities of the electron lines to be determined since in general, the time distributions of the contaminants differed.

3.3. SPIN ASSIGNMENTS

3.3.1. Previously Assigned States. Spin and parity assignments have been made on the basis of the γ-ray anisotropies, conversion coefficient measurements and a consideration of the transition strengths. The magnitudes of the angular distribution coefficients for transitions below the 290 ns isomer are attenuated due to de-orientation of the nuclei, with the attenuation becoming severe for the lowest states.

For the yrast transitions below the the isomer at 8854.6+Δ′ keV, the multipolarity assignments all support the previous measurements [1]). No new information was obtained on the 82 keV transition and the unobserved Δ and Δ′–Δ transitions since neither angular distribution nor electron conversion information was able to be extracted from the current experiments. The previous spin and parity assignments for the non-yrast states are also supported by the current measurement.

The A_2/A_0 ratio for the 536.3 keV transition has previously [1]) been measured to be -0.10(2), providing the basis for the spin 19/2 assignment of the state at 2114.1+Δ keV. The angular distribution was more severely attenuated in the current measurement (since more population proceeds through the high spin isomeric states than in the previous measurement), but the earlier value, in conjunction with the newly measured conversion coefficient, suggests a mixed E2/M1 assignment for the 536.3 keV transition with a mixing ratio of δ=-2.6.

The limit on the conversion coefficient for the 502.7 keV transition indicates a multipolarity of either E1 or E2. Taken with the previous measurement of a negative A_2/A_0 coefficient, which implies a dipole transition, a definite E1 assignment is possible. This gives positive parity for the spin 23/2 state at 2650.4+Δ keV, and also for the spin 25/2 state at 3117.4 keV due to the previous characterisation [1]) of the 467.0 keV transition as M1.

In the region between the yrast states with spins $35/2^+$ and $43/2^-$, the multipolarities of the strong 583.7 keV, 411.1 keV, 325.2 keV and 730.0 keV transitions assigned previously [1]) are supported by the current experiments.

The spin 45/2 state at 5733.8+Δ′ keV is confirmed to have negative parity with the identification of the multipolarities of both its feeding and de-exciting transitions (366.3 keV and 487.8 keV) as M2 and M1 respectively. Similarly, the 51/2 state at 6714.0+Δ′ keV has been assigned positive parity due to the 685.2 keV transition being identified as an M2 and the 613.7 keV transition as an M1. The 905.4 keV transition feeding the state at 7398.9+Δ′ keV has had its tentative M1 assignment [2]) confirmed by the current measurement.

3.3.2. New States. The revised placement of the 1068.9 keV transition has been complemented by the measurement of its multipolarity to be E2, thus establishing a $25/2^-$ state at $3216.6+\Delta$ keV. The coincidence relations show that this state must be fed in some manner from the $29/2^-$ state at $3243.4+\Delta$ keV, implying an unobserved 27 keV transition. The ratios of the three branches from the state at $3243.4+\Delta$ keV can be obtained from the relative intensities of the 511.5 keV, 1068.9 keV and 979.5 keV transitions in the spectrum gated on the 601.0 keV γ-ray, giving a 4.5(3) % branch through the unseen 27 keV transition. The calculated E2 conversion coefficient is ~4700 and this, combined with the measured mean life of the state at $3243.4+\Delta$ keV of 3.9(8) ns [4]), yields a partial mean life of 410(90) ns for the 27 keV γ-ray transition. This is close to the Weisskopf estimate of 366 ns.

Of the new states above the $63/2^-$ isomer, the yrast state at $9915.5+\Delta'$ keV has been assigned [5]) a spin and parity of $69/2^+$. The two transitions above this were too weak to yield any multipolarity information, but there are good reasons (based on structural arguments) for suspecting the 1166.4 keV transition to be a dipole. This will be discussed in the next section.

The electron conversion coefficient for the 292.6 keV transition is close to the M1 value. An E2 admixture is possible but the anisotropy of $A_2/A_0=0.16$ (12) is not sufficiently precise to distinguish between a $J\rightarrow J$ or $J\rightarrow(J-1)$ transition and hence the E2/M1 mixing ratio cannot be determined uniquely. A tentative assignment of $J^\pi = (63/2^-)$ to the state at $9149.2+\Delta'$ keV has been made. The alternative, a spin of 65/2, would make the state yrast and a significantly stronger population would then have been expected (at least equal to the population of the $65/2^+$ state at $9918.2+\Delta'$ keV).

The 1063.6 keV transition is a dipole transition from its anisotropy and of E1 character from the electron conversion coefficient, giving the spin and parity of the state at $9918.2+\Delta'$ keV as $65/2^+$. The 896.2 keV transition, which feeds $9918.2+\Delta'$ keV state, is tentatively assigned as an E2 from the conversion coefficient only, as the low intensity of this transition prohibited a measurement of its anisotropy.

Many new states have been discovered lower in the level scheme, and spins and parities assigned to some. The 308.9 keV transition de-exciting the level at 3426.3+Δ keV has a large negative anisotropy and its conversion coefficient is close to, but not quite consistent with, an M1 multipolarity (although this is a complex region of the spectrum). The 776.1 keV transition also de-exciting the same level has either an E1 or E2 multipolarity, giving a maximum spin for the 3426.3+Δ keV state of 27/2 and a probable assignment of $27/2^+$ considering also the 418.0 keV decay from the $31/2^+$ state.

The state at 3127.2+Δ keV is seen to be fed from the the state at 3243.4+Δ keV, which has a mean life of 3.9(8) ns [4]). The branching ratio, determined from the relative intensities of the 979.5 keV, 1068.9 keV and 511.5 keV transitions in the 601 keV gate, is 1.6(2) %. However, the non-observation of a 116 keV transition in this gate implies a conversion coefficient of at least 10 for such a transition and hence a multipolarity of M2, E3 or higher. The partial γ-ray mean life for a 116 keV M2 transition from the state at 3243.4+Δ keV is 14(3) μs, while that for an E3 is 24(6) μs. The Weisskopf estimates are 60 μs and 2.3 s for M2 and E3 multipolarities respectively. A 116 keV E3 transition would thus require an excessive enhancement over the single-particle E3 strength found in this region and can therefore be eliminated. Only the M2 possibility remains with a strength four times the Weisskopf value. Even for favoured M2 transitions (usually 0.5 – 1.0 W.u.), this is still a relatively large value which would require explanation. It is more probable that the 3127.2+Δ keV state is fed by a sequence of two or more unobserved lower multipolarity transitions.

In the region spanned by the 1319.9 keV E3 transition connecting the 5246.0+Δ keV and 3926.1+Δ keV states, there are six new levels, three of which have been assigned spins. The state at 4474.0+Δ keV is de-excited by a strongly anisotropic 548.0 keV transition with a conversion coefficient consistent with an M1 multipolarity, so the level is assigned as $37/2^+$. The 772.1 keV transition is then almost certainly M2 (however, no multipolarity information is available) as will be discussed in the next section. The anisotropy of the 278.1 keV transition indicates a stretched dipole and hence a spin of 37/2 for the state at 4961.0+Δ keV. Similarly the state at 5160.3+Δ keV is assigned a spin of 41/2 due to the negative A_2/A_0 of the 239.4 keV transition.

Higher in the scheme, the state at 6578.3+Δ′ keV is fed by a 136.1 keV transition which from its total conversion coefficient has E1 multipolarity, giving a spin and parity of 49/2⁻ for the state. The 478.0 keV transition which follows is probably an M2/E1 J→J mixed transition with a small quadrupole admixture to be consistent with the negative A_2/A_0 coefficient observed (the conversion coefficient for the transition could not be reliably determined due to the intensity being rather weak and because of its position in a complicated region of the spectrum).

The 880.0 keV transition which feeds the 51/2⁺ state at 6714.0+Δ′ keV is assigned as an M1 from the current data, giving the spin of the 7594.0+Δ′ keV level as 53/2⁺. The 903.7 keV transition which feeds the 49/2⁺ state at 6100.3+Δ′ keV is also an M1, leading to a spin and parity of 51/2⁺ for the level at 7004.0+Δ′ keV. The anisotropy for the 1324.6 keV transition which feeds that state constrains it to be a dipole, so the 8328.3+Δ′ keV level must have a spin of 53/2. Negative parity for this level is then given by the M1 assignment of the 929.4 transition which connects it to the 55/2⁻ state at 7398.9+Δ′ keV.

4. Discussion

The structure of the yrast states in ^{211}Rn has been detailed in previous publications. The characteristics of states which do not involve core excitations are well reproduced by shell model calculations [1]. Semi-empirical shell model calculations, which explicitly include the particle-vibration coupling to the 3⁻ octupole phonon are imperative to describe the core-excited states well [3,5,10]. In the high-spin region the structure of the states should be relatively simple due to the limited possibilities in forming states of the required angular momentum with the available valence particles. In this section the structure of some of the near-yrast states below the 63/2⁻ isomer, and the structure of the newly-discovered states above it, is discussed. Table 3 gives a summary of the configurations assigned to states in ^{211}Rn incorporating previous work and the new results.

4.1. STATES BELOW THE 63/2⁻ ISOMER AT 8854.6+Δ′ KEV

The possible structure of the 10 ns isomeric state at 2650.4+Δ keV has been commented upon previously [4] and with the assignment of even parity to the state, the suggested configuration of

$[\pi(h_{9/2}{}^3\, i_{13/2})_{11}\text{-}\ \nu(p_{1/2}{}^{-1})]_{23/2+}$ is supported. This is structurally similar to the isomeric 11^- states in ^{210}Rn [6]) and ^{212}Rn [7]) at 2563+Δ keV and 2761+Δ keV respectively. Each of these states decay primarily by an E1 transition, and in ^{210}Rn and ^{211}Rn a competing branch is also seen, as the partial level schemes given in figure 7 show. In ^{210}Rn this competing transition has been assigned as an E3 by its electron conversion coefficient value in conjuction with the (independently) assigned spins of its initial and final states. For the case of ^{212}Rn, an E3 decay of equal intensity to the E1 branch was seen by Lönnroth *et al* [11]), but was not observed in the measurement by Stuchbery *et al* [7]). Table 4 gives the transition strengths for the decay of these states. The similarity of the states in the different isotopes, seen from the similarity of the decay patterns, is apparent.

The 10^+ state at 2377+Δ keV in ^{210}Rn has an M1 de-exciting branch which is followed by a M1/E2 mixed transition. The tentative assignment of M1/E2 to the 536.3 keV transition de-exciting the $19/2^{(-)}$ level at 2114.1+Δ keV in ^{211}Rn provides evidence that the structure of that level corresponds to that of the 9^+ level at 2266+Δ keV in ^{210}Rn, dominated by the maximal coupling of a neutron-hole to a $\pi(h_{9/2}{}^4)_8$ component. Shell model calculations [1]) support this, with the configuration assigned being $\pi(h_{9/2}{}^4)_8\ \nu(f_{5/2}{}^{-1})$.

Further non-yrast states caused by occupation of higher energy neutron-hole orbitals exist above the $23/2^+$ level at 2650.4+Δ keV. The 467.0 keV M1 transition from the $25/2^+$ state at 3117.4+Δ keV is analogous to the 547.5 keV transition between the 12^- and 11^- states in ^{210}Rn. Immediately above these transitions there exists an 308.9 keV M1 transition in ^{211}Rn and a dipole 294.3 keV transition in ^{210}Rn. Competing with these transitions are less intense transitions which are probably E2 in character. The $25/2^+$ state and the state above are formed by the partial alignment of a neutron-hole with the proton configuration $(h_{9/2}{}^3\, i_{13/2})$ as can be seen by comparison with calculations made for ^{210}Rn [6]).

The $29/2^-$ state at 3243.4+Δ keV was previously identified [1]) as arising from the $\pi(h_{9/2}{}^3\, f_{7/2})_{14}+\ \nu(p_{1/2}{}^{-1})$ configuration. The non-yrast $25/2^-$ state at 3216.6+Δ keV to which it decays by a 27 keV E2 of strength ~1 Weisskopf unit (see section 3.3.2) is probably from the

$p_{1/2}^{-1}$ neutron-hole coupled to a 12^+ proton state arising from mixed $\pi(h_{9/2}^3\, f_{7/2})_{12^+}$ and $\pi(h_{9/2}^4)_{12^+}$ configurations. The observed separation of the 14_1^+ and 12_2^+ core states in ^{212}Rn [7] is 70 keV.

The region between yrast spin 31/2 and 43/2 in ^{211}Rn is complicated due to the competition of states based on the $(h_{9/2}^2\, i_{13/2}^2)$ and $(h_{9/2}^2\, i_{13/2}\, f_{7/2})$ proton configurations. The partial or full alignment of a neutron-hole to these states adds further complexity. The main decay of the $41/2^-$ state at 5246.0+Δ keV proceeds by a proton $i_{13/2}$ to $h_{9/2}$ transition, enhanced by coupling to the octupole vibration [3,12]. The competing decay is very fragmented, proceeding mainly via low multipolarity transitions.

Higher in the level scheme E3 transitions are a significant feature of the structure [1,2,3]. These are enhanced in strength by the coupling of the $i_{13/2} \rightarrow f_{7/2}$ proton and $j_{15/2} \rightarrow g_{9/2}$ neutron transitions to the octupole mode of the core [3,10]. Two M2 transitions of 685.2 keV (from the 7398.9+Δ′ keV state) and 366.3 keV (from the 6100.3+Δ′ keV state) with strengths of 0.6 (1) and 0.25 (3) Weisskopf single-particle units respectively are seen in competition with these E3 transitions (see table 2). These can be associated with a neutron $j_{15/2} \rightarrow i_{11/2}$ transition after considering the wave functions given by Poletti *et al* [10]. Empirical shell model calculations were made for the states involved and the results were consistent with the dominant configurations for the final states at 6714.0+Δ′ keV and 5733.8+Δ′ keV being $[\pi(h_{9/2}^3\, i_{13/2})_{17^-}\, \nu(i_{11/2})\, \nu_0^{-2}]_{45/2^-}$ and $[\pi(h_{9/2}^2\, i_{13/2}^2)_{20^+}\, \nu(i_{11/2})\, \nu_0^{-2}]_{51/2^+}$. Both M2 transitions are followed by M1 transitions which, from the configurations given in table 3, correspond to neutron $i_{11/2} \rightarrow g_{9/2}$ decays. This type of competition to E3 transitions between core-excited states is also expected in ^{210}Rn and ^{212}Rn; however there is less information on high-spin non-yrast states in these cases. A possible example is the 416 keV / 426 keV cascade in parallel with an 842 keV E3 transition between the states at 7310+Δ keV and 8469+Δ keV in ^{210}Rn [6] but the multipolarity of these cascade transitions has not yet been determined.

4.2. STATES ABOVE THE 63/2⁻ ISOMER AT 8854.6+Δ′ KEV

Eight new states that feed the 63/2⁻ isomer at 8854.6+Δ′ keV have been discovered. In order to clarify the structure of these states, semi-empirical shell model calculations have been made, yielding excitation energies of the states expected to lie in this region. In some cases the contribution of the coupling to the octupole mode of the core (the MPOC model) [5,10] have been included. In this section the results of the calculations are compared with experiment.

A detailed wavefunction for the 63/2⁻ isomer, which involves a double neutron core-excitation, is given by Poletti *et al* [10]. The diagonalization of the complete (13 × 13) matrix for this state yielded a set of levels, the lowest two of which are predicted to be at 8882 keV and 9176 keV [12], a difference of 294 keV. The observed state at 9149.2+Δ′ keV de-excites to the 63/2⁻ isomer via a 292.6 keV M1 or M1/E2 transition. The 9149.2+Δ′ keV state therefore may be a member of the 63/2⁻ "family". If it were, an E3 transition comparable in strength to the 687 keV transition is expected from the 9149.2+Δ′ keV 63/2⁻ state to the state at 8167.6+Δ′ keV. Thus one expects an E3 partial mean-life of 12 ns for the 9149.2+Δ′ keV state. Experimentally a limit of $\tau_m \leq 5$ ns is observed for this state and the E3 decay appears to be bypassed by a much faster M1 decay to the lower 63/2⁻ state. Such a decay is consistent with the proposition that both 63/2⁻ states arise from the same intrinsic configuration. (The Weisskopf estimate for this M1 is of the order 10^{-3} ns; and even l-forbidden M1 decays in this region are retarded by only 100).

The configuration of the 63/2⁻ isomer at 8854.6+Δ′ keV can be described approximately [5] by

$$| \pi(h_{9/2}^2 \tilde{i}_{13/2}^2)_{20+} \nu(\tilde{g}_{9/2} i_{11/2} f_{5/2}^{-1})_{23/2-} \nu(p_{1/2}^{-2})_{0+} |_{63/2-}$$

where the tilde indicates a coupling to the octupole mode of the core. There is only a limited number of ways to achieve higher spin states simply (i.e. with single-particle type excitations) without invoking further core excitation. The basic mechanisms forming yrast and near-yrast states are:

a) change of proton configuration from $\pi(h^2 i^2)_{20+}$ to $\pi(h\, i^3)_{21-}$,

b) change of neutron configuration from $\nu(g\, i)_{10+}$ to $\nu(g\, j)_{12-}$, $\nu(i\, j)_{13-}$, or $\nu(j^2)_{14+}$,

c) the maximal coupling of the $f_{5/2}$ neutron-hole.

d) excitation of the $i_{13/2}$ neutron-hole in place of the $f_{5/2}$ neutron-hole,

e) the breaking of the neutron-hole pair to, for example, $\nu(p^{-1} f^{-1})_{2,3}$

Mechanism a) is generally not effective as the excitation occurs at a cost of approximately 1.7 MeV for only one unit of spin gained. Neutrons are active structural components in this region, so mechanism b) is a favoured way of forming higher-spin states. However, the coupling of the neutron $j_{15/2} \rightarrow g_{9/2}$ transition to octupole vibrations is important when considering these states as will be commented on below. The $f_{5/2}$ neutron-hole is already present in many yrast configurations as $(f_{5/2})_{3/2}$ and full alignment of this component (mechanism c), normally costing between 500 keV and 1 MeV, may create yrast states in the high spin region where there are few alternatives. The excitation of the $i_{13/2}$ neutron-hole, mechanism d), is expensive in energy (typically 1 – 1.5 MeV), but allows very high spin states to be formed. However, these states may be difficult to observe as low-multipolarity single-particle decays are forbidden from this orbital. Experimentally we have no evidence for high-lying, long lived isomers. The final possibility given above, the breaking of the neutron-hole pair, is included in the calculations discussed below. Taking the two most effective mechanisms above, namely b) and e), the maximum spin obtainable is 77/2 from the configuration $\pi(h^2\, i^2)_{20+} \nu(j^2)_{14+} \nu(f^{-2}\, p^{-1})_{9/2-}$.

The semi-empirical shell model has been used to calculate the energies of yrast and near-yrast states above the $63/2^-$ isomer based on these mechanisms and the results of these calculations are shown in figure 8, along with the states observed in this energy region. Also shown are the results of MPOC calculations [5,10,12] for the isomeric $63/2^-$ and $69/2^+$ states at $8854.6+\Delta'$ keV and $9915.5+\Delta'$ keV respectively. (Note that the MPOC calculations yield a family of states, each of the same spin and parity).

In the semi-empirical shell model calculations the effect of the particle-vibration coupling to the octupole mode has not been explicitly considered in most cases, as the use of empirical two-nucleon matrix elements implicitly includes this effect. However, states involving the $(g_{9/2}\, j_{15/2})$ neutron pair (included in b) above) must receive special consideration. In states where this pair is maximally coupled, the octupole-coupled $g_{9/2}$ component of the empirical $j_{15/2}$ wave function is

completely blocked, causing the effective interaction between these nucleons to be significantly more repulsive than otherwise expected from empirical interactions [3,10]). An explicit treatment including the octupole vibration coupled components of the wave function is required in these cases. The interaction between the neutrons in this state and the $i_{13/2}$ proton is also affected, leading to more repulsive interactions (particularly in maximally aligned cases) and increased excitation energies. For these reasons the relative excitation energies of the states involving the $(g_{9/2}\, j_{15/2})$ neutron pair in ^{211}Rn are 1 MeV or more higher than states it is naively competitive with, e.g. those involving the $(i_{11/2}\, j_{15/2})$ neutrons. Therefore the $(g_{9/2}\, j_{15/2})$ states are not close to being yrast and are not shown in figure 8.

Above the $63/2^-$ isomer, there is only one likely configuration for the $65/2^+$ state at $9918.2+\Delta'$ keV. This configuration has the same components as that for the isomeric $69/2^+$ state at $9915.5+\Delta'$ keV but coupled to a lower total angular momentum. There is also only one positive parity 69/2 state (based on the same configuration) calculated near the tentatively assigned state at $10814.4+\Delta'$ keV.

The isomeric state at $9915.5+\Delta'$ keV has been discussed in a previous letter [5]). An MPOC calculation for this state yields the observed energy and de-exciting transition strength precisely.

In figure 8, there are three calculated 71/2 states close to the states observed at $11034.6+\Delta'$ keV and $11083.9+\Delta'$ keV. Confirmation of the observed states' spin and measurements of the parities would help to distinguish between the possibilities. Note also that there is only one calculated state (formed by the breaking of the neutron-hole pair to $p^{-1}\, f^{-1}$) with a spin of greater than 71/2 within one MeV of the state observed at $11234.1+\Delta'$ keV.

Finally, states based on the excitation of the $i_{13/2}$ neutron-hole (mechanism e above) appear at energies in excess of 12 MeV, as shown in figure 9. Competition with these configurations can be expected from a third core excitation. For example, the energy of the $73/2^-$ triple core-excited state $\pi(h^{-2}\, i^{2})\, \nu(i\, g^{2})\, \nu(f^{-2}\, p^{-2})$ is calculated to be 12086 keV.

5. Summary and conclusions

The level scheme of ^{211}Rn has been established to a spin of $69/2^+$ for yrast states and many near-yrast states have been observed. In considering the non-yrast states below spin 31/2, a similarity between the level schemes of the isotopes ^{210}Rn, ^{211}Rn and ^{212}Rn is noted. This is the result of the valence protons being the most active structural components in this region. In ^{210}Rn and ^{211}Rn, the partial alignment of neutron-holes also leads to states which are structurally similar.

Higher in the level scheme, M2/M1 cascades compete with strong E3 transitions. Configurations can be assigned to the intermediate states by noting that the neutron $j_{15/2} \rightarrow g_{9/2}$ (octupole-coupled) transition which gives rise to the E3 strength can proceed alternatively by $j_{15/2} \rightarrow i_{11/2}$ and $i_{11/2} \rightarrow g_{9/2}$ transitions in series.

For states above the $63/2^-$ isomer, semi-empirical shell model calculations have been made for all yrast and near-yrast states expected to occur before the next core excitation. Empirical configurations are suggested for those states whose spin and parity has been determined experimentally. The calculations indicate that the highest spin expected below 12 MeV (the energy predicted for a third core excitation) is 73/2 and a candidate for such a state is observed. This value is close to 77/2, the maximum reasonable spin available from the valence nucleons. To date, no high spin states involving the $i_{13/2}$ neutron-hole have been observed.

References

1) A.R. Poletti, G.D. Dracoulis, C. Fahlander and I. Morrison, Nucl. Phys. **A359** (1981) 180

2) G.D. Dracoulis, C. Fahlander and A.R. Poletti, Phys. Rev. **C24** (1981) 2386

3) A.R. Poletti, G.D. Dracoulis, A.P. Byrne, A.E. Stuchbery, S.J. Poletti, J Gerl and P.M. Lewis, Phys. Lett. **154B** (1985) 263

4) A.R. Poletti, G.D. Dracoulis, S.J. Poletti, A.P. Byrne, A.E. Stuchbery and J. Gerl, Nucl. Phys. **A442** (1985) 153

5) G.D. Dracoulis, P.M. Davidson, A.P. Byrne, B. Fabricius, T. Kibédi, A.M. Baxter, A.E. Stuchbery, A.R. Poletti and K.J. Schiffer, Phys. Lett. **246B** (1990) 31

6) A.R. Poletti, G.D. Dracoulis, C. Fahlander and I. Morrison, Nucl. Phys. **A380** (1982) 335

7) A.E. Stuchbery, G.D. Dracoulis, A.P. Byrne, A.R. Poletti, Nucl. Phys. **A486** (1988) 397

8) G.D. Dracoulis and A.P. Byrne, to be published.

9) T. Kibédi, G.D. Dracoulis, A.P. Byrne, Nucl. Instr. Meth. **A294** (1990) 523

10) S.J. Poletti, G.D. Dracoulis, A.R. Poletti, A.P. Byrne, A.E. Stuchbery and J. Gerl, Nucl. Phys. **A448** (1986) 189

11) T. Lönnroth, C.W. Beausang, D.B. Fossan, L. Hildingsson, W.F. Peil, Jr., E.K. Waburton, Phys. Scripta **39** (1988) 56

12) S.J. Poletti, M.Sc thesis, Australian National University (1985), unpublished

Figure Captions

Fig. 1. Level scheme of ^{211}Rn determined in this and previous works [1,2,4]). The width of the arrows represents the γ-ray intensity observed. Where the γ-ray energy is enclosed in parentheses the transition was not observed, but the existence of a decay path is required by the coincidence data. The positions of levels shown with dotted lines is uncertain as the order of the feeding an de-exciting transitions may be reversed. Mean lives are shown to the right of the level energy.

Fig. 2. Representative prompt spectra for some yrast cascade transitions.

Fig. 3. Early spectra for two yrast cascade transitions, showing transitions occurring above the isomers at 5246+Δ′ keV and 6100+Δ′ keV. In the top panel, the 487 keV line is a contaminant.

Fig. 4. Spectra showing γ-rays coincident with the 1068.9 keV transition. The top panel shows γ-rays occurring within ±24 ns. The bottom panel is a composite spectrum obtained from subtracting the spectrum observed to be late with respect to the gating transition from that observed to be early. Here "early" corresponds to a time range from 24 ns to 812 ns before the gating transition, and "late" to the same range after the gating transition. See text for further discussion.

Fig. 5. The top panel shows a sum of early spectra (gated on the 1299 keV, 769 keV and 687 keV γ-rays) showing transitions above the 290 ns isomer. Only those lines common to the three component spectra are labelled (the contribution of a contaminant from a 685 keV line in ^{208}Po has been removed by subtracting the early gate of a coincident transition in ^{208}Po). The middle and lower panels show background subtracted prompt spectra for the 1061 keV and 1166 keV transitions, showing the clear relationship between the transitions and the 150 keV line. (The 407 keV peak seen in all three panels is from remnant random coincidences with the ^{198}Pt Coulomb excitation line.)

Fig. 6. Totalised spectra for the γ-rays and conversion electrons. The electron spectrum has been shifted so that the K-shell transitions in radon align with the corresponding γ-ray.

Fig. 7. Partial level schemes of ^{210}Rn and ^{211}Rn. See text for discussion.

Fig. 8. Excitation energies of states observed above the $63/2^-$ isomer compared to those calculated with the MPOC and semi-empirical shell models. For the semi-empirical shell model calculations, the energies have been adjusted downward by 270 keV so that the calculated $63/2^-$ state is at the same energy as the observed state.

Table 1: Gamma-rays observed in ^{211}Rn.

Energy (keV) [a]	Intensity	Multipolarity	A_2/A_0	Initial State (keV)
81.7	55 (8)	E2		3926.1+Δ
113.9	1 (0.2) [d]			[b]
119.6	235 (11)	E2	-0.04 (3)	1577.8+Δ
120.8	1.5 (0.5) [d]			1698.6+Δ [c,e]
132.7	7 (2) [d]		0.02 (19)	4474.0+Δ [c]
132.8	1.4 (0.6) [d]			4550.9+Δ
136.1	15 (5) [d]	E1	-0.20 (9)	6714.0+Δ′
146.8	5 (1) [d]	D [f]	-0.22 (12)	8758.0+Δ′ [c]
150.2	1.4 (0.3) [d]			11234.1+Δ′ [c]
169.8	1.2 (0.3) [d]			[b]
220.2	1.3 (0.4) [d]			11034.6+Δ′
239.4	13 (1)	D [f]	-0.22 (6)	5160.3+Δ [c]
278.9	10 (2) [d]	D [f]	-0.19 (6)	5239.8+Δ
282.9	5 (2) [d]	D [f]	-0.35 (11)	8611.2+Δ′ [c]
292.6	8 (1) [d]	(M1)	0.16 (12)	9149.2+Δ′
308.9	7 (2) [d]	M1	-0.41 (23)	3426.3+Δ
325.2	220 (20)	E1	0.10 (2)	5246.0+Δ
339.9	2.7 (0.6) [d]			[b]
366.3	27 (3)	M2	0.30 (9)	6100.3+Δ′
410.7	20 (4) [d]			4961.0+Δ
411.1	137 (35)	M1	-0.07 (5)	4920.9+Δ
415.1	23 (5) [d]			4341.2+Δ
415.4	6 (3) [d]			2114.1+Δ [c]
418.0	18 (3)			3844.4+Δ
430.0	3.6 (0.4) [d]			[b]
467.0	31 (2)	M1	-0.33 (7)	3117.4+Δ
478.0	30 (2)	(M2/E1)	0.40 (12)	6578.3+Δ′
487.8	58 (5)	M1	-0.33 (6)	5733.8+Δ′
492.0	8 (2) [d]		0.13 (11)	4418.1+Δ
502.7	47 (3)	E1	-0.03 (7)	2650.4+Δ
511.5	700 (10)	E2	0.16 (2)	3243.4+Δ
531.6	5 (1)			8161.9+Δ′
536.3	158 (4)	(E2/M1)	0.02 (5)	2114.1+Δ
537.1	11 (3)			8167.6+Δ′
539.9	1000	E2	0.15 (2)	539.9
548.0	47 (10)	M1	-0.64 (7)	4474.0+Δ
569.9	709 (9)	E2	0.14 (2)	2147.7+Δ

Energy (keV) [a]	Intensity	Multipolarity	A_2/A_0	Initial State (keV)
584.2	709 (13)	E2		2731.9+Δ
601.0	674 (9)	E1	-0.09 (3)	3844.4+Δ
613.7	73 (1)	M1	-0.90 (6)	6714.0+Δ′
624.7	8 (2) [d]			4550.9+Δ
630.6	38 (2)		0.38 (18)	3874.0+Δ [c]
685.2	40 (2)	M2	0.28 (13)	7398.9+Δ′
687.0	128 (4)	E3	0.10 (4)	8854.6+Δ′
730.0	120 (2)	E1	-0.10 (4)	5239.8+Δ
732.2	2.3 (0.5) [d]			[b]
758.3	10 (2)			8925.9+Δ′
768.7	160 (3)	E1	-0.10 (3)	8167.6+Δ′
772.1	11 (4)			5246.0+Δ
773.1	7 (4)			9627.7+Δ′
776.1	11 (1)	(E2)	0.12 (14)	3426.3+Δ
854.3	442 (7)	E3	0.21 (3)	6100.3+Δ′
880.0	22 (2)	M1	-0.28 (13)	7594.0+Δ′
896.2	6.1 (0.8) [d]	(E2)		10814.4+Δ′
903.7	54 (3)	M1	-0.44 (7)	7004.0+Δ′
905.4	35 (4)	M1	-0.97 (10)	8304.3+Δ′
916.3	32 (3)			7630.3+Δ′
916.5	3.6 (0.8) [d]			[b]
918.3	979 (7)	E2	0.10 (2)	1458.2
929.4	25 (1)	M1	-0.77 (7)	8328.3+Δ′
952.2	4 (1) [d]			[b]
979.5	30 (1) [d]		0.13 (8)	3127.2+Δ
994.7	33 (1)	(E2)	-0.14 (9)	4920.9+Δ
1034.9	10 (1)	(D) [f]	-0.32 (22)	4961.0+Δ
1060.9	31 (1)	E3	0.45 (9)	9915.5+Δ′
1063.6	14 (1)	E1	-0.37 (18)	9918.2+Δ′
1068.9	38 (1)	E2	0.23 (8)	3216.6+Δ [c]
1072.6	1.4 (0.5) [d]			2650.4+Δ
1156.0	3.4 (0.6) [d]			[b]
1166.4	6 (4) [d]			11083.9+Δ′ [c]
1298.6	215 (2)	E3	0.27 (3)	7398.9+Δ′
1319.9	255 (2)	E3	0.23 (3)	5246.0+Δ
1324.6	13 (2)	(D) [f]	-0.58 (15)	8328.3+Δ′

[a] Uncertainties in γ-ray energies are of the order of 0.2 keV.

[b] Transition is unplaced in the level scheme but must be above the isomer at 8854.6+Δ′.

[c]) Placement is ambiguous, see figure 1.

[d]) Intensity estimated from coincidence measurement.

[e]) The position of the level is uncertain as the order of the feeding and de-exciting transitions may be reversed.

[f]) D - Dipole.

Table 2: Conversion coefficients and multipolarities determined from the current experiment [a]).

E (keV)	Type	Experiment	Assigned	Theory
136.1	T	0.5 (3)	E1	0.2
146.8	T	0.2 (5)	E1	0.2
		or 1.1 (6)		
292.6	K	0.55 (8)	(M1)	0.55
308.9	K	0.8 (1)	(M1)	0.5
366.3	K	1.0 (1)	M2	0.9
	L	0.24 (2)		0.22
	M	0.08 (1)		0.06
487.8	K	0.20 (1)	M1	0.14
502.7	K	<0.04	E1	E1: 0.009
				M1: 0.159
536.3	K	0.032 (4)	(M1/E2)	M1: 0.108
				E2: 0.021
548.0	K	0.15 (5)	M1	0.10
613.7	K	0.11 (2)	M1	0.08
	L	0.046 (9)		0.010
685.2	K	0.19 (4)	M2	0.14
	L	0.07 (1)		0.03
776.1	K	<0.01	(E2)	E1: 0.005
				E2: 0.01
880.0	K	0.028 (3)	M1	0.030
896.2	K	0.012 (3)	(E2)	0.008
903.7	K	0.044 (4)	M1	0.028
	L	0.008 (1)		0.005
905.4	K	0.033 (5)	M1	0.028
929.4	K	0.032 (5)	M1	0.026
	L			
994.7	K	0.0082 (6)	E2	0.0065
1060.9	K	0.0121 (7)	E3	0.0124
	L	0.0033 (3)		0.0036
	M	0.0011 (2)		0.0009
1063.6	K	0.004 (2)	E1	0.002
1068.9	K	0.0063 (14)	E2	0.0057
1324.6	K	<0.06		

[a]) See ref. [1] for transitions previously determined.

Table 3: Table of nominal configurations [a]) for states in ^{211}Rn.

Energy (keV)	J^{π}	Nominal Configuration [a])
0.0	1/2−	$\pi(h^4)_{0+} \nu p^{-1}$
539.9	5/2−	$\pi(h^4)_{0+} \nu f^{-1}$
1458.2	9/2−	$\pi(h^4)_{4+} \nu p^{-1}$
1577.8	13/2−	$\pi(h^4)_{6+} \nu p^{-1}$
1577.8+Δ	17/2−	$\pi(h^4)_{8+} \nu p^{-1}$
(1698.6+Δ)	(15/2−)	$\pi(h^4)_{8+} \nu p^{-1}$?
2114.1+Δ	19/2(−)	$\pi(h^4)_{8+} \nu f^{-1}$
2147.7+Δ	21/2−	$\pi(h^4)_{8+} \nu f^{-1}$
2650.4+Δ	23/2+	$\pi(h^3 i)_{11-} \nu p^{-1}$
2731.9+Δ	25/2−	$\pi(h^4)_{12+} \nu p^{-1}$
3117.4+Δ	25/2+	$\pi(h^3 i)_{11-} \nu f^{-1}$
3127.2+Δ	(25/2+)	$\pi(h^3 i)_{10-} \nu f^{-1}$?
3216.6+Δ	25/2−	$\pi(h^3 f)_{12+} \nu p^{-1} \otimes \pi(h^4)_{12+} \nu p^{-1}$
3243.4+Δ	29/2−	$\pi(h^3 f)_{14+} \nu p^{-1}$
3426.3+Δ	27/2+	$\pi(h^3 i)_{11-} \nu f^{-1}$
3844.4+Δ	31/2+	$\pi(h^3 i)_{15-} \nu p^{-1}$
3874.0+Δ		
3926.1+Δ	35/2+	$\pi(h^3 i)_{17-} \nu p^{-1}$
(4341.2+Δ)		
4418.1+Δ		
4474.0+Δ	37/2+	$\pi(h^3 i)_{17-} \nu f^{-1}$
4509.8+Δ	37/2+	$\pi(h^3 i)_{16-} \nu f^{-1}$
4550.9+Δ		
4920.9+Δ	39/2+	$\pi(h^3 i)_{17-} \nu f^{-1}$
4961.0+Δ	37/2	$\pi(h^2 i f)_{17-} \nu f^{-1}$?
5160.3+Δ	41/2	$\pi(h^2 i f)_{18-} \nu f^{-1}$?
5239.8+Δ	39/2−	$\pi(h^2 i^2)_{19+} \nu p^{-1}$
5246.0+Δ	41/2−	$\pi(h^2 i^2)_{20+} \nu p^{-1}$
5246.0+Δ′	43/2−	$\pi(h^3 i)_{17-} \nu g (p^{-2})_{0+}$ [b])
5733.8+Δ′	45/2−	$\pi(h^3 i)_{17-} \nu i (p^{-2})_{0+}$
6100.3+Δ′	49/2+	$\pi(h^3 i)_{17-} \nu j (p^{-2})_{0+} \otimes \pi(h^2 i^2)_{20+} \nu g (p^{-2})_{0+}$ [b])
6578.3+Δ′	49/2−	
6714.0+Δ′	51/2+	$\pi(h^2 i^2)_{20+} \nu i (p^{-2})_{0+}$
7004.0+Δ′	51/2+	$\pi(h^2 i f)_{18-} \nu j (p^{-2})_{0+}$?
7398.9+Δ′	55/2−	$\pi(h^2 i^2)_{20+} \nu j (p^{-2})_{0+}$ [b])

Energy (keV)	J^π	Nominal Configuration [a]
7594.0+Δ′	53/2+	$\pi(h^2 i^2)_{20+} \nu(i f^{-1} p^{-1})$ or $\pi(h^2 i^2)_{20+} \nu(g f^{-2})$?
7630.3+Δ′		
8161.9+Δ′		
8167.6+Δ′	57/2+	$\pi(h^3 i)_{17-} \nu(g i f^{-1})(p^{-2})_{0+}$ [b]
8304.3+Δ′	57/2−	$\pi(h^2 i^2)_{20+} \nu(j f^{-1} p^{-1})$ or $\pi(h^2 i^2)_{20+} \nu(j f^{-2})$?
8328.3+Δ′	53/2−	$\pi(h^2 i^2)_{20+} \nu j (p^{-2})_{0+}$ or $\pi(h^2 i^2)_{20+} \nu(j f^{-1} p^{-2})$?
8611.2+Δ′		
8758.0+Δ′		
8854.6+Δ′	63/2−	$\pi(h^3 i)_{17-} \nu(j i f^{-1})(p^{-2})_{0+} \otimes$ $\pi(h^2 i^2)_{20+} \nu(g i f^{-1})(p^{-2})_{0+}$ [b]
8925.9+Δ′		
9149.2+Δ′	(63/2)−	$\pi(h^3 i)_{17-} \nu(j i f^{-1})(p^{-2})_{0+} \otimes$ $\pi(h^2 i^2)_{20+} \nu(g i f^{-1})(p^{-2})_{0+}$ [b]
9627.7+Δ′		
9915.5+Δ′	69/2+	$\pi(h^2 i^2)_{20+} \nu(j i f^{-1})(p^{-2})_{0+}$
9918.2+Δ′	65/2+	$\pi(h^2 i^2)_{20+} \nu(j i f^{-1})(p^{-2})_{0+}$
10814.4+Δ′	(69/2+)	$\pi(h^2 i^2)_{20+} \nu(j i f^{-1})(p^{-2})_{0+}$ [c]
11034.6+Δ′	(71/2)	$\pi(h^2 i^2)_{20+} \otimes \nu(j i f^{-1} p^{-2})$ or $\nu(j^2 f^{-1} p^{-2})$ or $\nu(j i f^{-2} p^{-1})$ [c]
11083.9+Δ′	(71/2)	
11234.1+Δ′	(73/2)	$\pi(h^2 i^2)_{20+} \nu(j i f^{-2} p^{-1})$ [c]

a) The leading configuration(s) in the wave functions are given. For protons $h \equiv h_{9/2}$, $i \equiv i_{13/2}$, $f \equiv f_{7/2}$. For neutrons, $g \equiv g_{9/2}$, $i \equiv i_{11/2}$, $j \equiv j_{15/2}$ and for neutron-holes $p \equiv p_{1/2}{}^{-1}$, $f \equiv f_{5/2}{}^{-1}$.

b) For detailed wavefunctions, see ref [10].

c) Possible configurations based on tentative spin given.

Table 4: Selected transition strengths in ^{210}Rn [a], ^{211}Rn [b] and ^{212}Rn [c].

	Nucle s	$I_f \rightarrow I_i$	Energy (keV)	B(EL) (e^2fm^{2L})
E1	^{210}Rn	$11^- \rightarrow 10^+$	185	8.2×10^{-7}
	^{211}Rn	$23/2^+ \rightarrow 21/2^-$	503	$5.0\ (3) \times 10^{-7}$
	^{212}Rn	$11^- \rightarrow 10^+$	106	$4.7\ (2) \times 10^{-5}$
E3	^{210}Rn	$11^- \rightarrow 8^+$	897	7.7×10^3
	^{211}Rn	$23/2^+ \rightarrow 17/2^-$	1073	$3\ (1) \times 10^3$
	^{212}Rn	$11^- \rightarrow 8^+$	1067 [d]	$< 8 \times 10^3$ [e]

[a] From [4], no errors quoted.

[b] Lifetime of state at 2650.4+Δ keV from [1], branching ratios from this paper.

[c] From [5].

[d] Transition not observed experimentally.

[e] Limit from limit on γ-ray intensity.

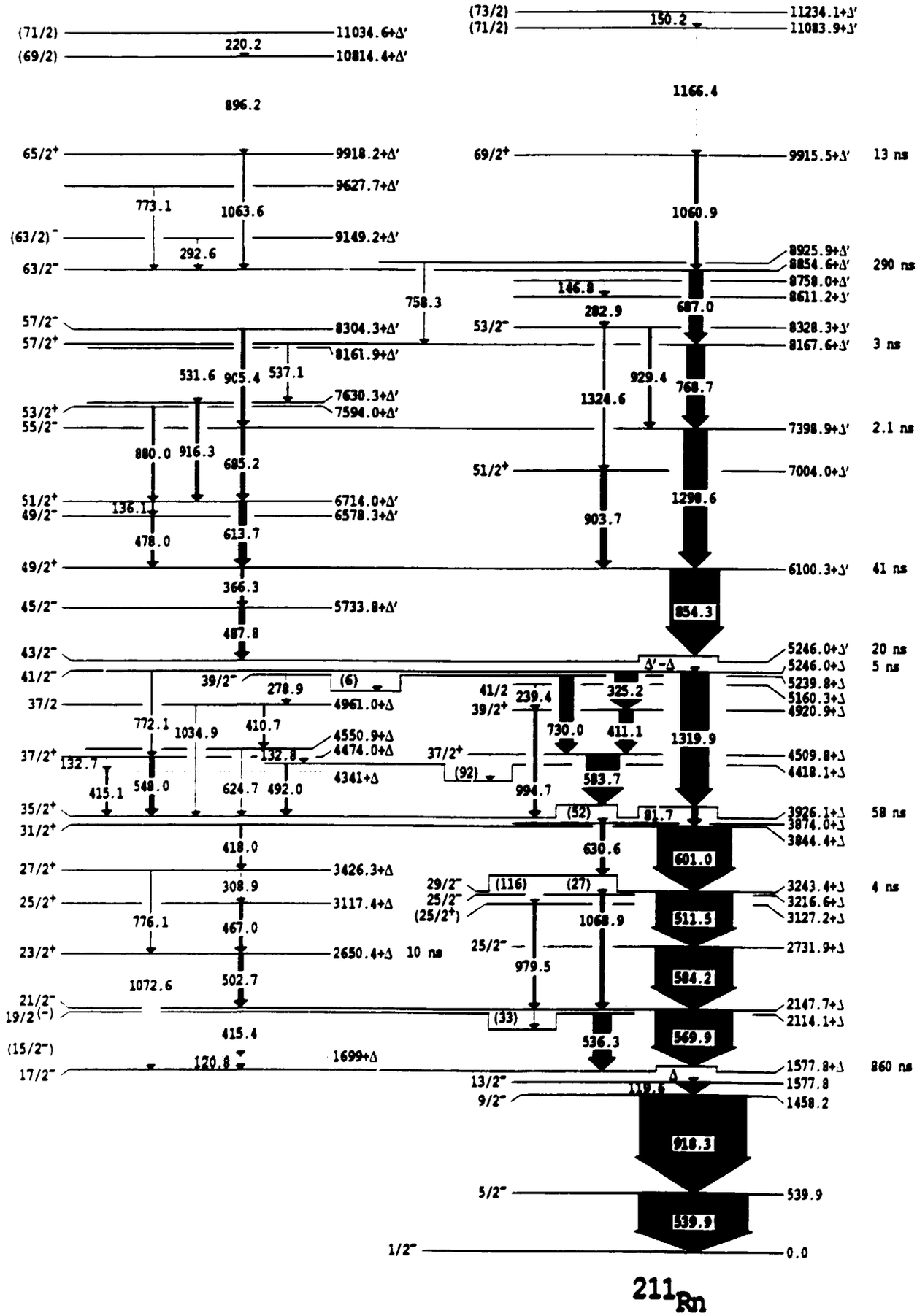
(73/2) 11234.1+Δ'
(71/2) 11083.9+Δ'
150.2
(71/2) 11034.6+Δ'
220.2
(69/2) 10814.4+Δ'
1166.4
896.2
65/2+ 9918.2+Δ'
69/2+ 9915.5+Δ' 13 ns
9627.7+Δ'
773.1
1063.6
1060.9
(63/2)- 9149.2+Δ'
292.6
8925.9+Δ'
63/2- 8854.6+Δ' 290 ns
8758.0+Δ'
146.8
8611.2+Δ'
758.3
282.9
687.0
57/2- 8304.3+Δ'
53/2- 8328.3+Δ'
57/2+ 8161.9+Δ'
8167.6+Δ' 3 ns
531.6
905.4
537.1
929.4
768.7
1324.6
7630.3+Δ'
53/2+ 7594.0+Δ'
55/2- 7398.9+Δ' 2.1 ns
880.0
916.3
685.2
51/2+ 7004.0+Δ'
1290.6
51/2+ 6714.0+Δ'
136.1
49/2- 6578.3+Δ'
903.7
478.0
613.7
49/2+ 6100.3+Δ' 41 ns
366.3
45/2- 5733.8+Δ'
854.3
487.8
43/2- 5246.0+Δ' 20 ns
Δ'-Δ
41/2- 5246.0+Δ 5 ns
39/2- (6)
278.9
41/2 239.4
325.2
5239.8+Δ
37/2 4961.0+Δ
39/2+ 5160.3+Δ
772.1
1034.9
410.7
730.0
411.1
1319.9
4920.9+Δ
4550.9+Δ
37/2+ 4474.0+Δ
132.7
132.8
37/2+ 4509.8+Δ
(92)
4418.1+Δ
4341+Δ
415.1
548.0
624.7
492.0
994.7
583.7
35/2+ (52) 81.7 3926.1+Δ 58 ns
3874.0+Δ
31/2+ 3844.4+Δ
418.0
630.6
601.0
27/2+ 3426.3+Δ
29/2- (116) (27) 3243.4+Δ 4 ns
308.9
25/2+ 3117.4+Δ
25/2- 3216.6+Δ
(25/2+) 1068.9 511.5 3127.2+Δ
776.1
467.0
25/2- 2731.9+Δ
23/2+ 2650.4+Δ 10 ns
979.5
584.2
1072.6
502.7
21/2- 2147.7+Δ
19/2(-) (33) 2114.1+Δ
415.4
536.3
569.9
(15/2-)
120.8
1699+Δ
17/2- 1577.8+Δ 860 ns
Δ
13/2- 1577.8
9/2- 1458.2
918.3
5/2- 539.9
539.9
1/2- 0.0
211Rn

Figure 1.

Figure 2.

counts (x 100)
0
50
100
0
4
8
0
10
20
30
energy (kev)
500
1000
Rn & Pt X-Rays
147
239
279
283
325
411
478
512
536
570
584
601
614
687
730
769
854
904
995
1299
1320
239
279
325
360
(407)
411
467
503
512
584
601
631
730
854
1069
1320
488
512
536
570
584
601
614
631
687
769
854
1299
570 keV prompt
1320 keV prompt
854 keV prompt
• 211At

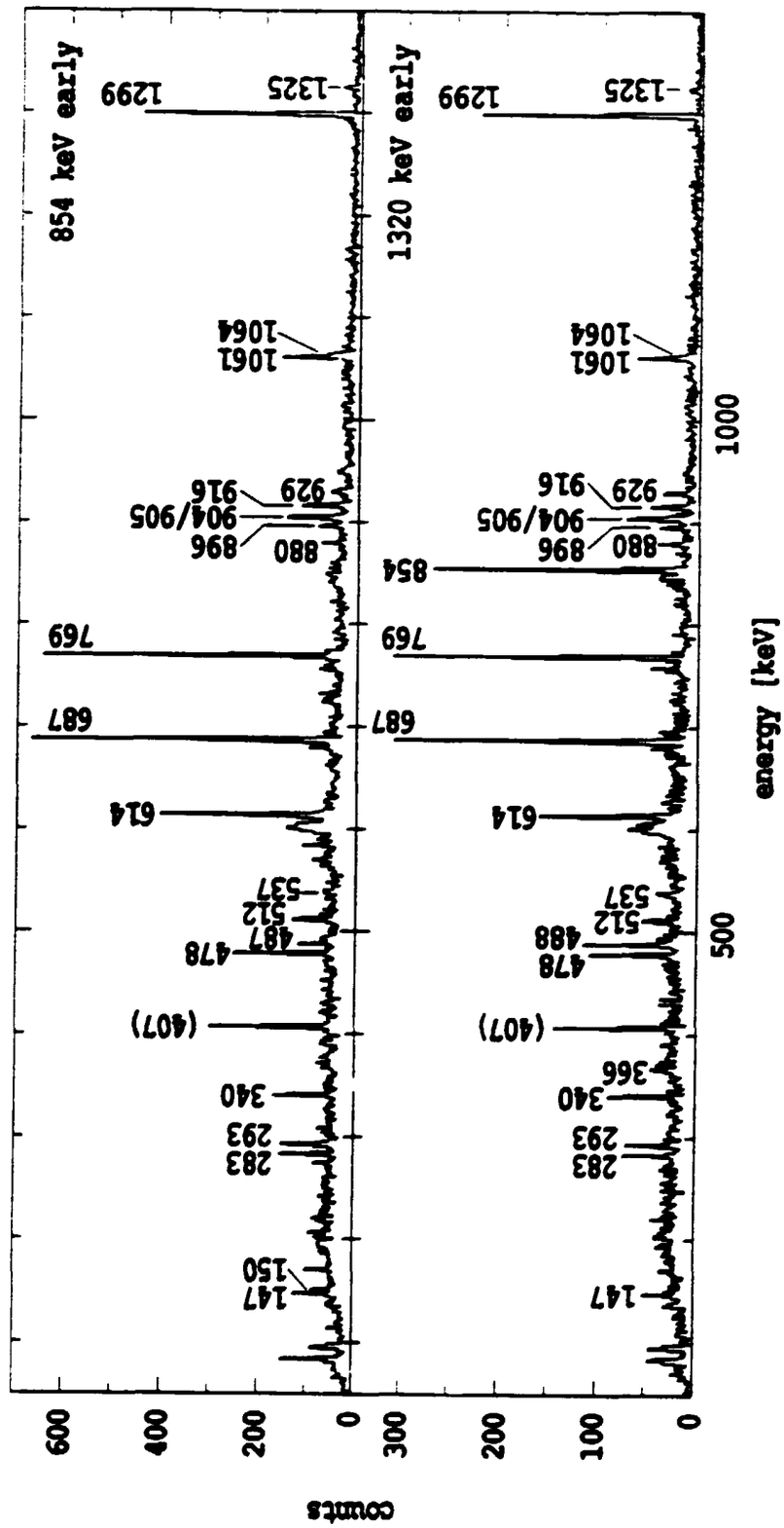
854 keV early
1320 keV early
1325
1299
1064
1061
929
916
904/905
896
880
854
769
687
614
537
512
488
478
(407)
366
340
293
283
147
150
1000
500
energy [keV]
600
400
200
0
300
200
100
0
counts

Figure 3.

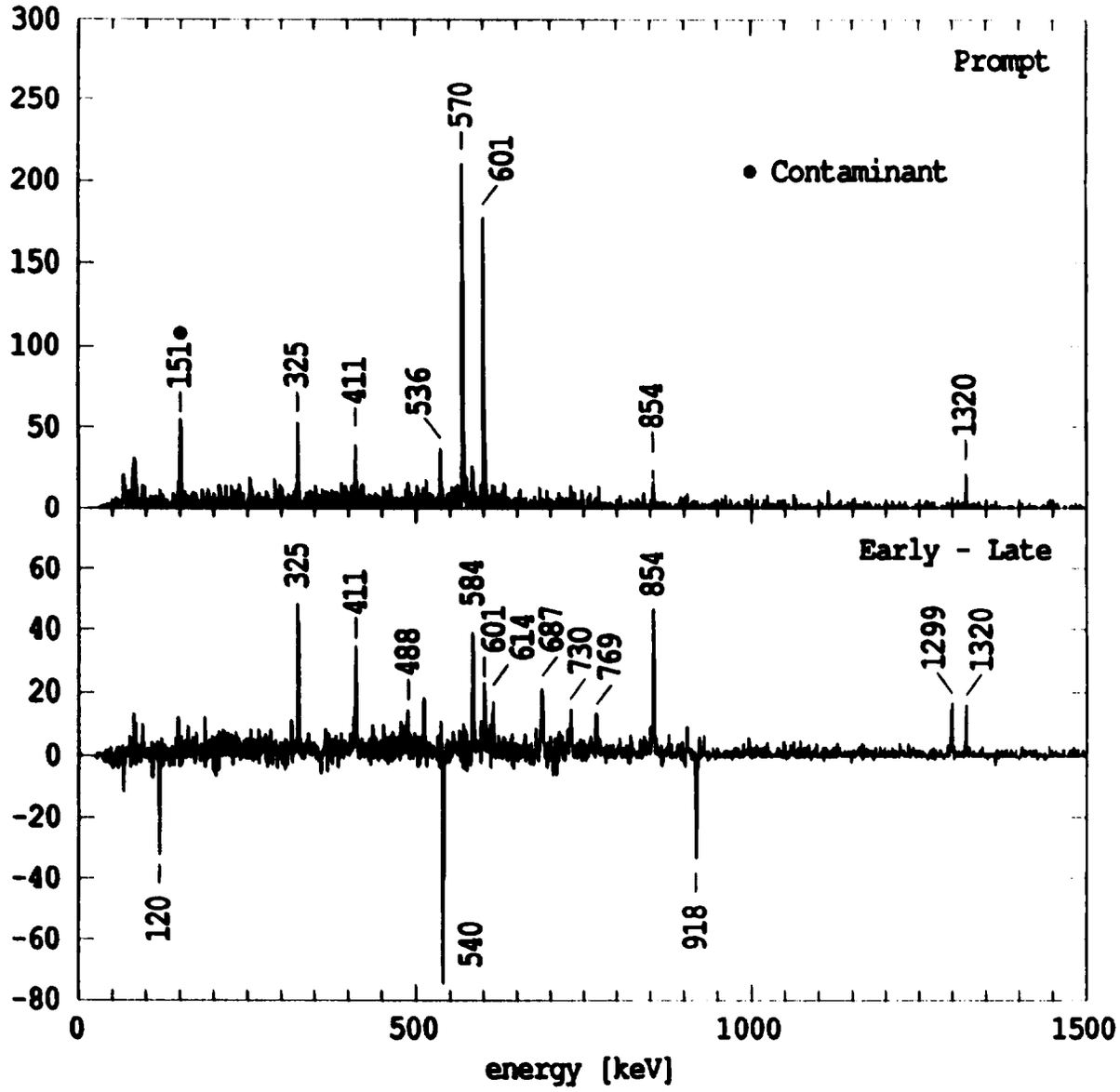
Prompt
• Contaminant
151•
325
411
536
570
601
854
1320
Early - Late
325
411
488
584
601
614
687
730
769
854
1299
1320
120
540
918
counts
energy [keV]
300
250
200
150
100
50
0
60
40
20
0
-20
-40
-60
-80
0
500
1000
1500

Figure 4

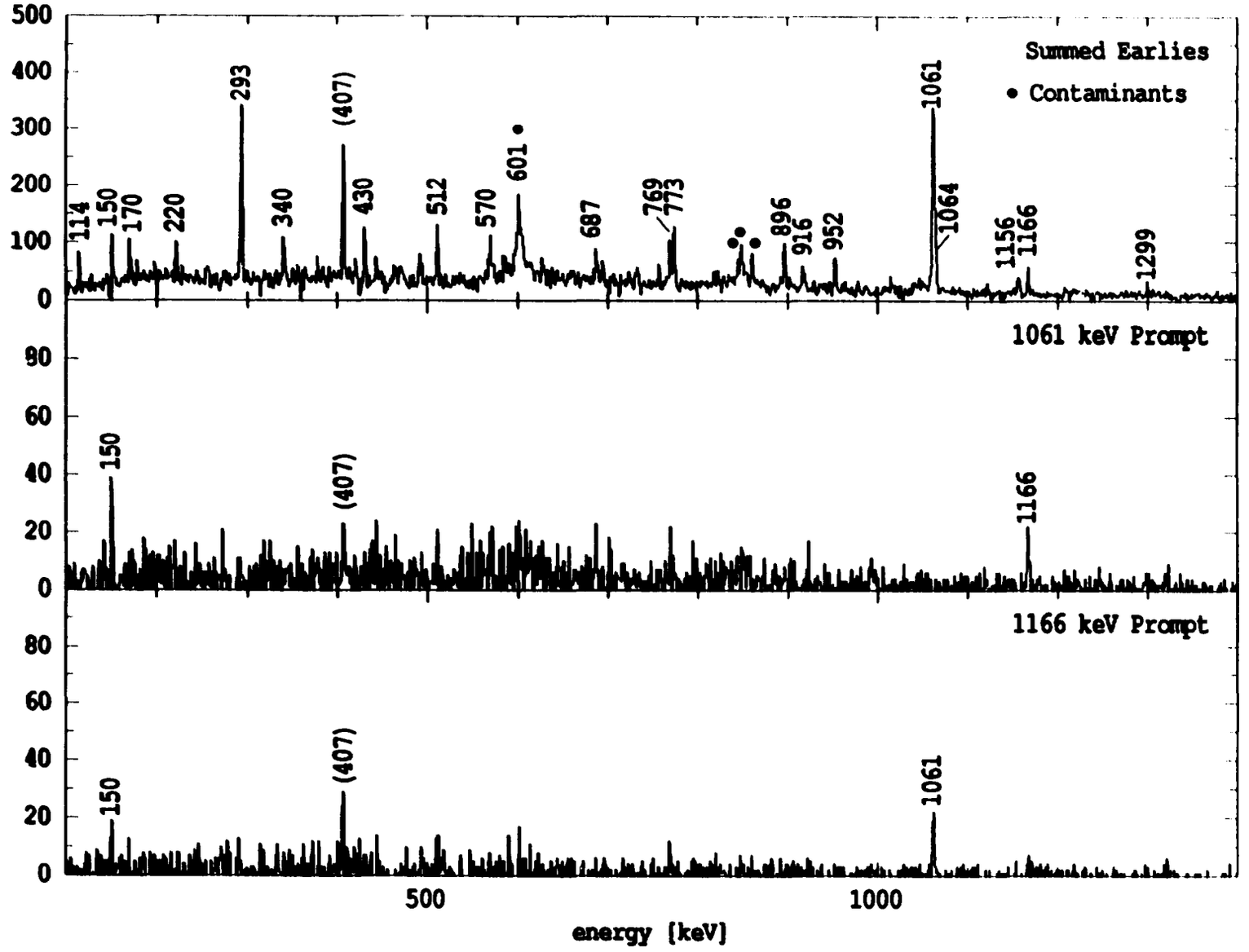
Summed Earlies
• Contaminants
1061 keV Prompt
1166 keV Prompt
counts
energy [keV]
500
1000
114
150
170
220
293
340
(407)
430
512
570
601 •
687
769
773
896
916
952
1061
1064
1156
1166
1299

Figure 5.

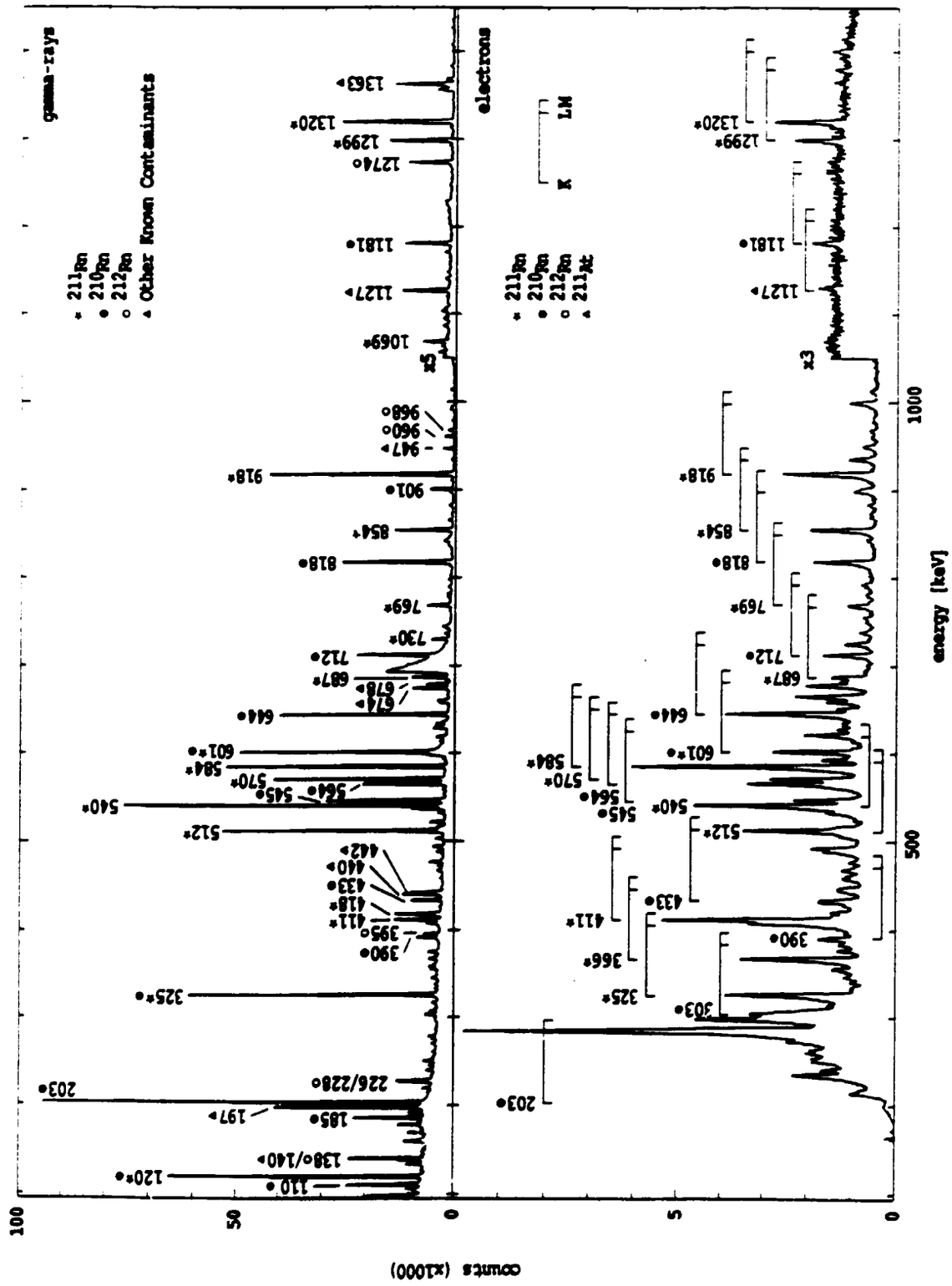
gamma-rays
electrons
Other Known Contaminants
energy [keV]
counts (x1000)
x5
x3
1000
500
100
50
0
5
0

Figure 6.

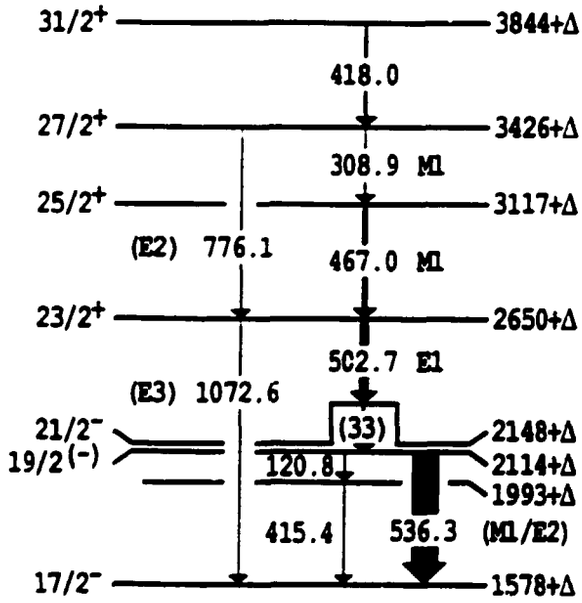

^{211}Rn

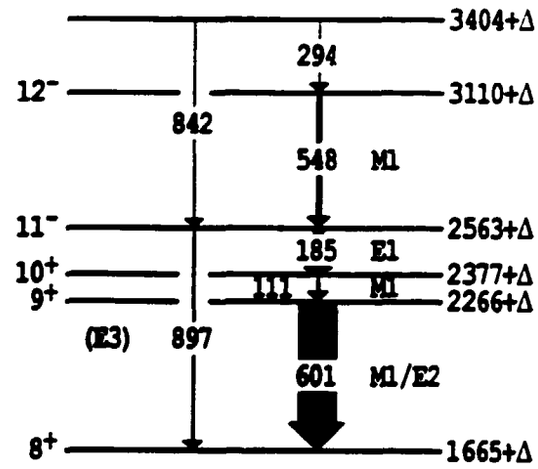

^{210}Rn

Figure 7.

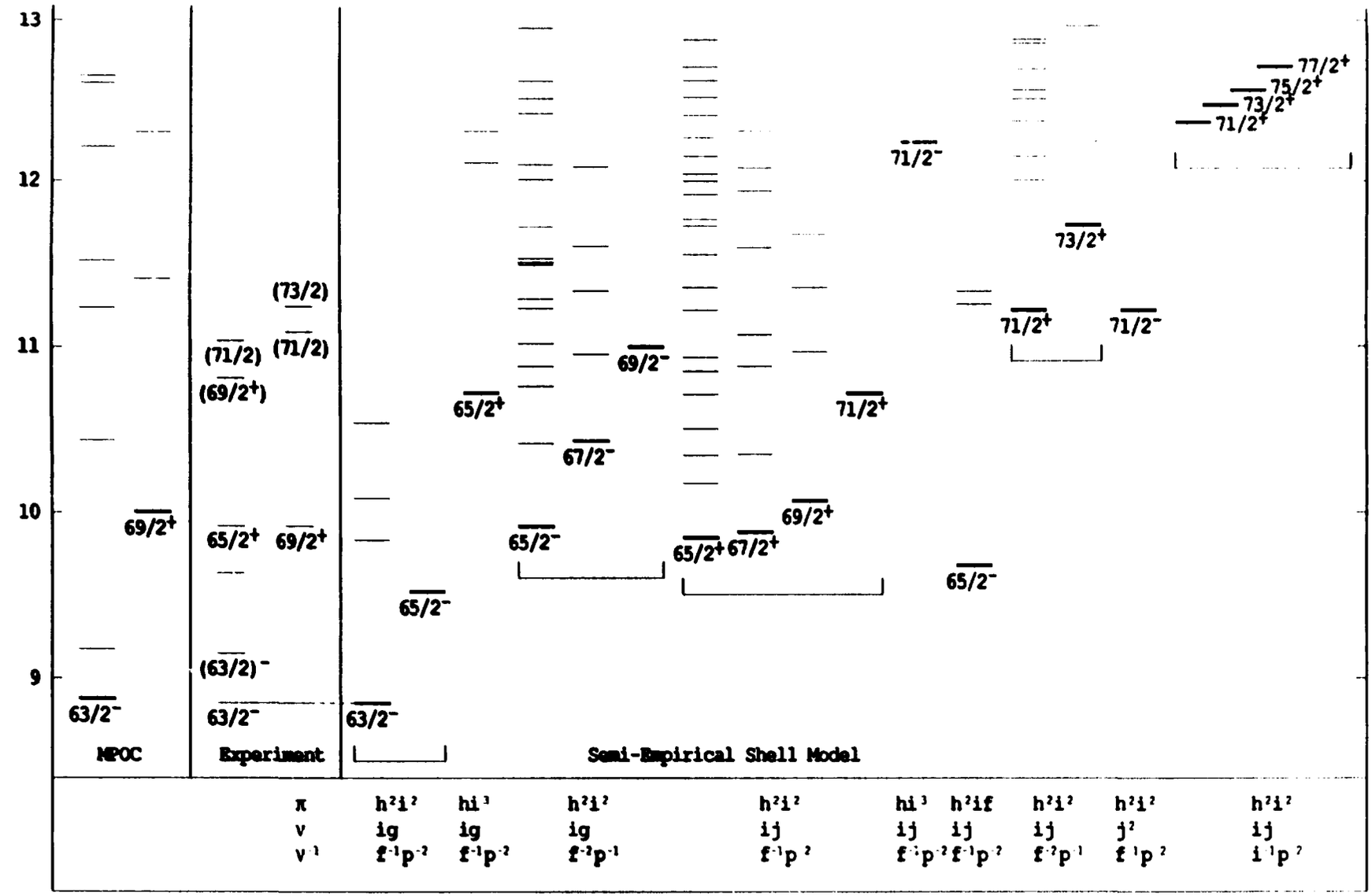
Energy (MeV)
13
12
11
10
9
63/2⁻
69/2⁺
MPOC
(63/2)⁻
63/2⁻
65/2⁺
69/2⁺
(69/2⁺)
(71/2)
(73/2)
(71/2)
Experiment
63/2⁻
65/2⁻
65/2⁺
67/2⁻
69/2⁻
65/2⁻
65/2⁺
67/2⁺
69/2⁺
71/2⁺
71/2⁻
65/2⁻
71/2⁺
71/2⁻
73/2⁺
71/2⁺
73/2⁺
75/2⁺
77/2⁺
Semi-Empirical Shell Model
π h²i² hi³ h²i² h²i² hi³ h²if h²i² h²i² h²i²
ν ig ig ig ij ij ij ij j² ij
ν⁻¹ f⁻¹p⁻² f⁻¹p⁻² f⁻²p⁻¹ f⁻¹p² f⁻¹p⁻² f⁻¹p² f⁻²p⁻¹ f⁻¹p² i⁻¹p²

Figure 8.